Available online at www.sciencedirect.com
SCIENCE DIRECT
Applied Catalysis A: General 310 (2006) 105–113
APPLIED CATALYSIS A: GENERAL
www.elsevier.com/locate/apcata

Formation of high surface area Li/MgO—Efficient catalyst for the oxidative dehydrogenation/cracking of propane

C. Trionfetti, I.V. Babich, K. Seshan *, L. Lefferts

Catalytic Processes and Materials, Faculty of Science and Technology, IMPACT University of Twente, P.O. Box 217, 7500AE Enschede, The Netherlands

Received 24 February 2006; received in revised form 16 May 2006; accepted 17 May 2006
Available online 30 June 2006

Abstract

In this study nanoscale clusters of Li/MgO oxide with varying lithium contents are prepared *via* the sol–gel method. The preparation routine consists of co-gelation of $LiNO_3$ and $Mg(OCH_3)_2$ in methanol/water solution followed by drying at 50 °C under vacuum and calcination at 500 °C in air. The structural and textural transformations that take place during oxide formation are studied with TGA–DSC–MS and FTIR spectroscopy. The obtained materials are characterized by TEM, N_2 physisorption and XRD. Presence of increasing amounts of lithium precursor causes extensive hydrolysis of the alkoxide sol. Appreciable amounts of lithium ions can be incorporated in the magnesia gel even under the mild conditions during sol–gel transformation. Non-incorporated lithium ions form a separate carbonate phase, which has a detrimental effect on the surface area due to enhanced sintering. The Li/MgO oxide materials thus prepared possess high surface area (50–190 m^2/g) depending on Li content. Small amounts of lithium ions, when present as a dispersed phase, do not seem to influence the structural and textural characteristics of the magnesia gel and, in these cases, nanoscale Li/MgO oxide clusters with high surface areas similar to pure MgO can be prepared. Sol–gel derived Li/MgO provides significantly higher olefin yields in ODH of propane in comparison with conventional Li/MgO catalysts, especially at lower temperatures.

Keywords: Sol–gel Li/MgO; Nanoscale oxide; Oxidative dehydrogenation

1. Introduction

Oxides, in which defects act as catalytic sites, attract considerable attention as catalysts in processes involving oxidation reactions [1–3]. Oxidative dehydrogenation (ODH) is an example. ODH is an exothermic reaction, converts alkanes such as ethane or propane to olefins (ethylene, propylene) from which a variety of polymers and chemicals are made. The process has definite advantages over conventional dehydrogenation basically due to the presence of oxygen which prevents coking and overcomes thermodynamic equilibrium limitation [4].

Despite being an attractive possibility, the efforts focused on the redox-type ODH catalyst systems gave low yields (e.g., <30% propene yield from propane) due to total combustion to carbon oxides [5]. On the other hand non-redox[1] catalysts, such as Li/MgO mixed oxides, are reported in literature as promising catalytic systems for oxidative dehydrogenation and cracking of LPG, C_2–C_4 range alkanes, due to their high activity and selectivity towards olefins formation (>50% yields) [6–8]. This study focuses on oxidative dehydrogenation/cracking of propane; the term ODH is used though for convenience.

Defect sites are reported to play a key role in Li/MgO catalyst and $[Li^+O^-]$ type defect sites are considered to be responsible for the catalytic activity [9,10]. Li/MgO materials prepared conventionally, e.g., by impregnation of MgO with aqueous solution of Li salts followed by drying and calcination, are generally characterized by low surface areas [11]. It was shown that for MgO (90 m^2/g), incorporation of Li caused substantial loss of surface area of Li/MgO (2 m^2/g) after heat treatment at 650 °C [11]. This is mainly caused by: (i) high temperature treatments necessary to build Li into the MgO lattice to create active sites [12] and (ii) alkali compounds facilitating sintering. As a result these catalysts have low activity. Enhancement of the surface area and defect site ($[Li^+O^-]$) concentration can help to improve activity of the Li/MgO catalysts and operate at lower temperatures. In

* Corresponding author. Tel.: +31 534893254; fax: +31 534894683.
E-mail addresses: K.Seshan@tnw.utwente.nl, k.seshan@utwente.nl (K. Seshan).

[1] Non-redox catalysts are defined here as catalysts that do not allow change in the valence of the metal ions; consequently oxygen ions are not removed under reaction.

0926-860X/$ – see front matter © 2006 Published by Elsevier B.V.
doi:10.1016/j.apcata.2006.05.029

order to achieve this, preparation of small oxide clusters in the nanometer range would be needed; spherical nanoparticles of 3 nm contain 50% of atoms or ions in the surface [13]. Such high surface area Li/MgO materials could be appropriate for ODH reactions, in contrast to oxidative coupling of methane, since the temperature of operation is much lower (<600 °C) than for the latter (>750 °C) [14,15].

Sol–gel method is suitable for preparing MgO oxides, as extensively discussed by Klabunde and co-workers [16], and homogeneous Li/MgO mixed oxides [17]. Typically MgO oxides thus obtained possess high surface area. The mild conditions during the formation of the hydroxide/oxide networks in gel result in porous and well dispersed systems. In the case of Li/MgO the doping is done by co-gelling a lithium salt and the magnesia precursor [18]. In this study attempts are made to prepare oxide clusters of Li/MgO *via* the sol–gel method and to understand the structural and textural transformations that take place during oxide formation. Simultaneously we aim at achieving high incorporation of Li in the MgO lattice under mild temperatures. The catalytic performance of sol–gel derived catalysts is compared with conventionally prepared Li/MgO.

2. Experimental

2.1. Materials

Commercially available $Mg(OCH_3)_2$ solution (Aldrich, 8.7 wt.%, in methanol), methanol (Merck) and $LiNO_3$ (Merck) were used. Water added to the solution was double de-ionized.

2.2. Catalysts preparation

A solution of $Mg(OCH_3)_2$ in methanol (0.4 M) containing $LiNO_3$ (in appropriate amounts to obtain 0, 1, 3 and 5 wt.% Li in MgO) was mixed with water in methanol (0.8 M) at room temperature and allowed to stand for 24 h for gelation (wet gels). After drying at 50 °C in vacuum for 7 h the dried gels were calcined at 500 °C in air for 1 h.

2.3. Characterization of gel/oxide

The composition of the samples was determined by chemical analysis (AAS). X-ray diffraction patterns were recorded by a Philips PW1830 diffractometer using Cu Kα radiation, $\lambda = 0.1544$ nm. XRD patterns were measured in reflection geometry in the 2θ range between 20° and 50°. N_2 adsorption measurements were carried out using a Micrometrics Tristar instrument. The samples were out-gassed in vacuum at 200 °C for 24 h prior to the analysis.

FTIR measurements were conducted using a Fourier transform spectrometer, Nicolet 20 XSB. In all experiments 10 mg of dried gel or oxide was mixed with KBr (catalyst: KBr ratio 1–4) and pressed into a disk. The disk was placed in a cell, heated up to 100 °C and purged with air, before recording IR spectra at the desired temperatures.

The thermal analysis of the gels was done using a Setaram TGA–DSC 111, heating rate 5 °C/min in air. Gases evolved during these measurements were analysed with mass spectrometry (QMS-Omnistar). Transmission electron microscopy (Philips CM30) was used to determine the size and shape of the particles.

2.4. Catalytic test

Sol–gel Li/MgO samples were calcined at 500 °C for 1 h, pressed, crushed and sieved to 0.3–0.35 mm particles. Catalytic tests were carried out in a fix-bed reactor (quartz tube, internal diameter 4 mm) in the range of temperature between 500 and 650 °C. The catalyst bed (50 mg) was packed between two quartz–wool plugs. Before each catalytic test the catalysts had been pretreated in O_2/He flow (30 ml/min, 1 h) at temperature 50 °C higher than the reaction temperature. The feed consisted of 10% propane, 10% oxygen, 2% carbon dioxide and balance helium. Carbon dioxide has been added to the feed in order to achieve a constant CO_2 concentration over the whole catalyst bed, as CO_2 has an inhibiting effect upon the reaction. The total flow rate was 100 ml/min. A Varian 3800 GC was used to analyse all the gases.

Impregnated Li/MgO catalysts have been tested under the same conditions.

3. Results

3.1. Characterization of the gels

3.1.1. Magnesia gel

Fig. 1a shows the result of TGA in air for a sample of magnesia gel (Mg-gel) obtained from hydrolysis of $Mg(OCH_3)_2$. The small weight loss of 3% observed below 100 °C is associated to residual methanol and water still present in the dried gel. This was typical for TGA profiles of all the gels recorded and will not be discussed further. The experimental weight loss of 34%, between 300 and 350 °C, corresponds to the decomposition of Mg-gel. Fig. 1b shows the analysis of gases evolved during the above TGA experiment as followed by mass spectrometry. Evolution of CO_2 in the temperature range corresponding to the weight loss in TGA indicates combustion of the organic species. Fig. 1c shows the DSC signal in air recorded during the gel decomposition. Two exothermic transitions are observed in the temperature ranges 200–250 and 300–350 °C, respectively. For the first peak there is no corresponding weight loss in TGA (see Fig. 1a) and it should represent an isomorphic transformation. The second exothermic peak at 350 °C corresponds to the combustion of the alkoxide gel.

Fig. 2 shows infrared spectra of gels treated at different temperatures. Fig. 2a represents the spectrum obtained from the Mg-gel at 100 °C. In this case, peaks characteristic for –OH stretching (3600–3700 cm^{-1}) and $-CH_3$ stretching (2700–

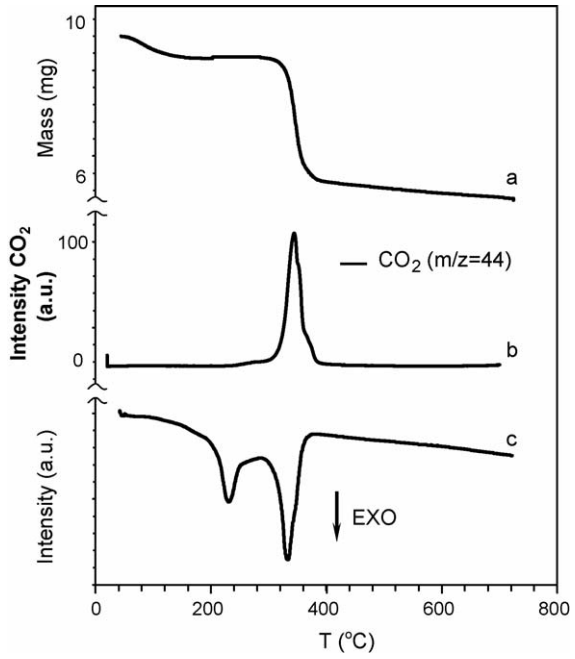

Fig. 1. Thermogravimetric analysis of magnesium gel (a); analysis of gases produced followed by mass spectrometer (b); differential scanning calorimetry data during the TGA experiments. Flow air 30 ml/min, temperature ramp 5 °C/min.

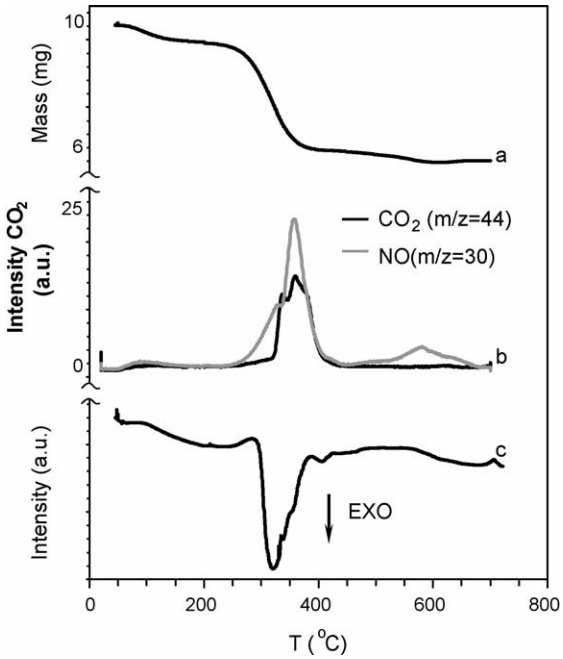

Fig. 3. Thermogravimetric analysis of 1 wt.% Li–Mg-gel (a); analysis of gases produced followed by mass spectrometer (b); and differential scanning calorimetry during the TGA experiment (c). Flow air 30 ml/min, temperature ramp 5 °C/min.

2900 cm^{-1}, methoxy groups) as well as a broad band between 3600 and 3400 cm^{-1} due to hydrogen bond formation are detected. As expected from the TGA/DSC data above, the methoxy groups should decompose below 350 °C and thus were not observed in FTIR spectrum of the sample calcined at 500 °C (Fig. 2b).

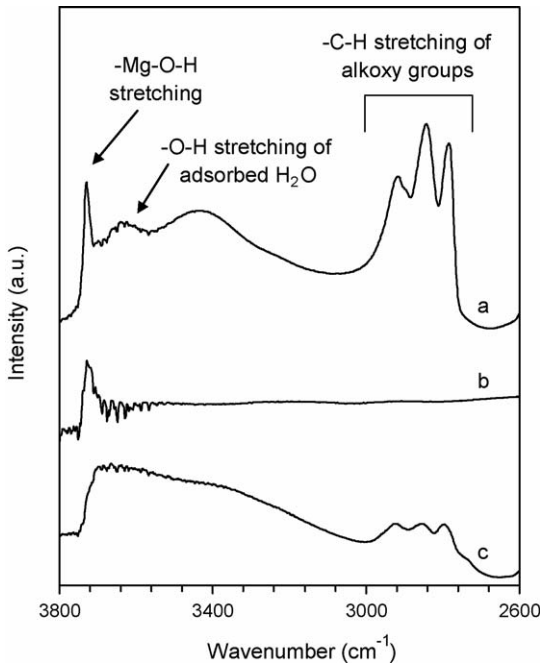

Fig. 2. IR spectra of Mg-gel heated to 100 °C in air (a), Mg-gel heated to 500 °C (b) and 5 wt.% Li–Mg-gel heated to 100 °C (c).

3.1.2. Li containing magnesia gel

Figs. 3 and 4 show the details of thermal analyses of two Li containing magnesia gels (Li–Mg-gel), i.e., 1 and 5 wt.% Li, respectively. The TGA profile for 1 wt.% Li–Mg-gel was similar to that obtained for Mg-gel; the weight loss corresponded to 33% (Fig. 3a) and occurred in a single step

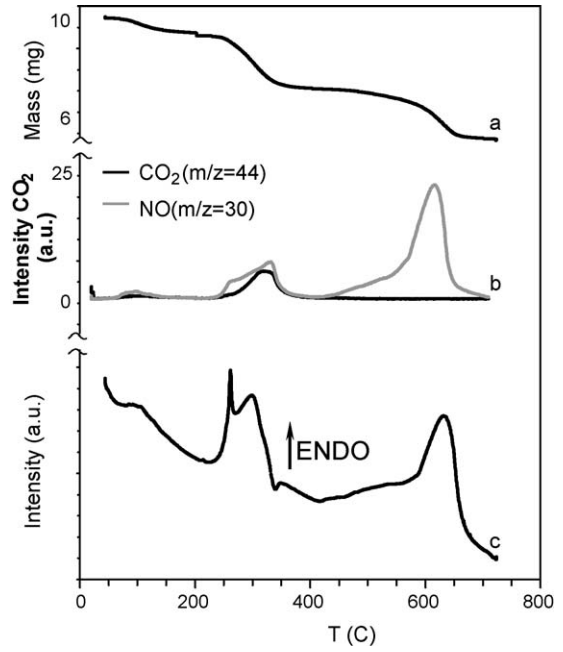

Fig. 4. Thermogravimetric analysis of 5 wt.% Li–Mg-gel (a); analysis of gases produced followed by mass spectrometer (b); differential scanning calorimetry during the TGA experiment (c). Flow air 30 ml/min, temperature ramp 5 °C/min.

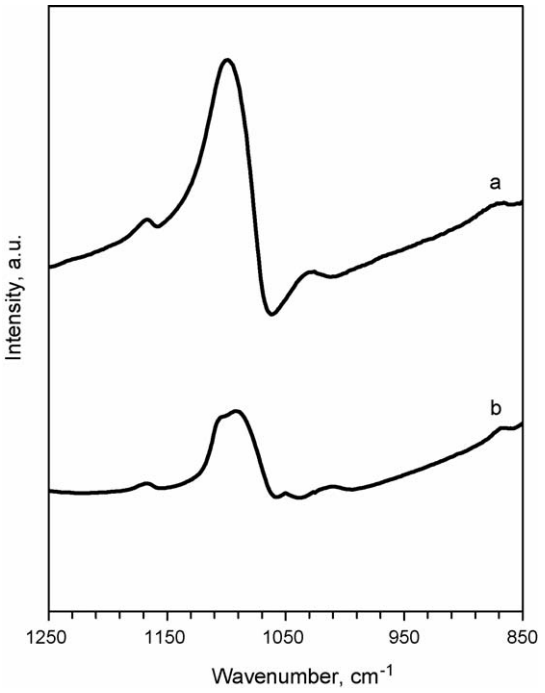

Fig. 5. FTIR of dried gels: Mg-gel (a) and 5 wt.% Li–Mg-gel (b). Spectra have been taken at $T = 100$ °C. The signal at 1100 cm^{-1} is related to the bending of Mg–O–Mg bond.

between 300 and 350 °C. In the case of 5 wt.% Li–Mg-gel (Fig. 4a) two regions of weight losses were recorded: the first weight loss (27%) was observed around 300 °C and the second (24%) at 650 °C. Figs. 3b and 4b show MS analyses of evolved gases for 1 and 5 wt.% Li–Mg-gel during the TG experiments. The CO_2 signal corresponding to the gel combustion was observed in both cases (300–350 °C). However, it has to be noted that both the temperature of CO_2 evolution and the peak shape are different in the case of 5 wt.% Li–Mg-gel, indicating that the nature of gel was different.

Additionally, two NO peaks around 350 and 650 °C (originating from decomposition of nitrate species present in gel) were observed with MS. The NO peak at 350 °C is typical for $Mg(NO_3)_2$ decomposition [19]. Since the starting precursors for Li–Mg-gel were $Mg(OCH_3)_2$ and $LiNO_3$, some magnesium nitrate is apparently formed during gelation. Decomposition of bulk $LiNO_3$ was found around 650 °C and, hence, the second NO peak observed is assigned to decomposition of unreacted $LiNO_3$ present in the gel. For the 5 wt.% Li–Mg-gel, the intensity of the NO peak at 650 °C is much higher. The corresponding TGA weight loss at 650 °C (24%, Fig. 4a,) indicates that about 60% of Li added was present as free $LiNO_3$ in the gel.

Table 1
BET surface areas for samples obtained using the sol–gel method, after calcination at 500 °C for 1 h

Samples	BET (m^2/g)
MgO	250
1 wt.% Li/MgO	190
3 wt.% Li/MgO	70
5 wt.% Li/MgO	50

Figs. 3c and 4c show the DSC in air for the two lithium containing magnesia gels. In both Li containing gels, the isomorphic transition, observed for pure magnesia gel $T < 250$ °C, was absent. For the 1 wt.% Li–Mg-gel, one exothermic peak (320 °C) corresponding to gel combustion was recorded (Fig. 3c). In contrast, for the 5 wt.% Li–Mg-gel two endothermic peaks were seen between 250–320 and at 630 °C (Fig. 4c). The first DSC signal between 250 and 320 °C is typical for bulk $Mg(NO_3)_2$ decomposition. These two endothermic transitions therefore correspond to decomposition of Mg and Li nitrates, respectively.

For the 5 wt.% Li–Mg-gel sample, the exothermic peak corresponding to alkoxide gel combustion (Fig. 1c) was not observable for two reasons: (i) the endothermic $Mg(NO_3)_2$ decomposition occurs in the same temperature range and overlaps with the exothermic signal and (ii) the alkoxide content of the gel was low. In agreement, the infrared spectra of the 5 wt.% Li–Mg-gel (Fig. 2c) showed much less intense $-CH_3$ stretching vibration. This also implies that the extent of hydrolysis in this sample is much higher.

Fig. 5 shows the IR spectra of the gels in the range 850–1250 cm^{-1}, i.e., the region typical for Mg–O–Mg bending vibrations [17]. The band at 1100 cm^{-1} is related to the presence of Mg–O–Mg bonds. The signal decreases when lithium is present in the Mg–gel (see Fig. 5b).

3.2. Characterization of oxide materials (Li/MgO)

Table 1 hows the BET surface areas of oxide powders obtained after calcination of the gels at 500 °C. Two important conclusions could be drawn: (i) high surface area materials could be made by the sol–gel method and (ii) even in the presence of Li, for sol–gel Li/MgO oxide samples, high surface area (190 m^2/g) could be maintained in comparison to materials prepared conventionally (<10 m^2/g). However, at higher lithium concentration (5 wt.%) the resulting surface area is less spectacular.

XRD patterns of the oxide samples are shown in Fig. 6. The peaks corresponding to MgO phase became narrower for samples with higher lithium loading. From the X-ray line broadening analysis (XLBA) we estimated particle size of 5 nm in the case of MgO and this increased up to 10 nm for 5 wt.% Li/MgO sample. In the case of samples containing higher amounts of lithium, peaks of Li_2CO_3 could also be observed. No other phases of Li, including $LiNO_3$, were detected by XRD.

Semi-quantitative experiments were carried out with X-ray powder diffraction in order to estimate the amount of lithium present as a separate phase (Li_2CO_3) and thus to evaluate the amount of lithium incorporated into the lattice of MgO (solid solution). In Fig. 7, the relative intensity of the strongest line [0 0 2] of Li_2CO_3 and [2 0 0] of MgO is plotted for mechanical mixtures of Li_2CO_3–MgO[2] and for sol–gel Li/MgO samples.

[2] XRD detection limit for bulk Li_2CO_3 in mechanical mixture with MgO is below 0.1 wt.% Li.

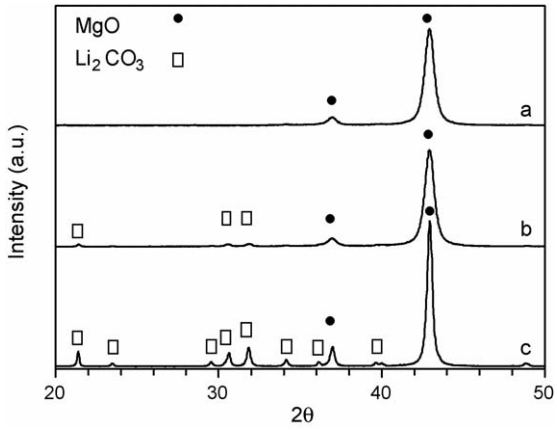

Fig. 6. XRD pattern for pure MgO (a), 1 wt.% Li/MgO (b) and 5 wt.% Li/MgO (c).

The differences between the data for mechanical mixtures and for the synthesized sol–gel samples with the same composition correspond to the amounts of lithium incorporated into MgO lattice. Based on these observations we can estimate the amount of Li incorporated into MgO lattice – 40% for 1 wt.% Li, 25% for 3 wt.% and 16% for 5 wt.% Li in MgO. This means that solid solution in sol–gel Li/MgO samples is already formed under mild conditions, i.e., by co-gelling $Mg(OCH_3)_2$ and $LiNO_3$ and calcination at 500 °C.

Fig. 8a shows the influence of calcinations temperature on the surface areas. For the 1 wt.% Li/MgO sample, high surface area could be maintained even after the thermal treatment at 700 °C. Pore size distribution for 1 and 5 wt.% Li/MgO samples does not change even after treatment at 700 °C. TEM data (not presented here) show only a slight increase in the particle size in line with BET results. For the sample with 5 wt.% Li, thermal treatment had a drastic influence on the surface area; this may be due to the fact that the sample contained a considerable amount of free Li_2CO_3. In order to check this, samples of 1 wt.% Li prepared by sol–gel method and wet impregnation of MgO (Li present as $LiNO_3$) were subjected to similar thermal treatments. MgO used for impregnating $LiNO_3$ was the same high surface material prepared with the sol–gel route. It can be seen from Fig. 8b that indeed: (i) Li when present as a free phase before calcinations affects surface area drastically with increase in temperature and (ii) this influence is minimized when most of Li is built into the MgO lattice, i.e., in the case of sol–gel method samples.

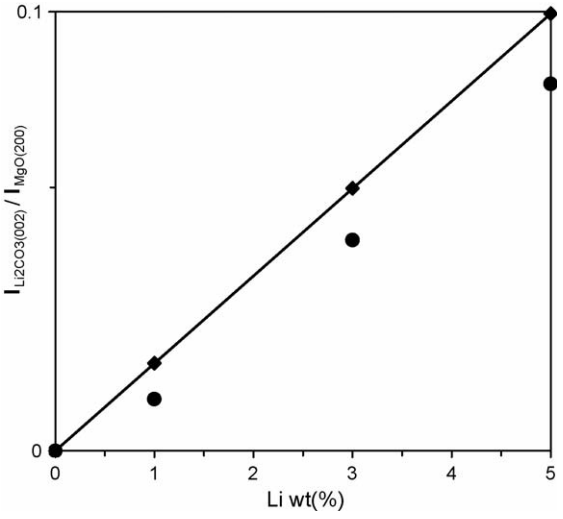

Fig. 7. Ratio between peak area of Li_2CO_3 and MgO in standard mechanical mixtures (■) and for Li/MgO samples obtained by sol–gel method (●).

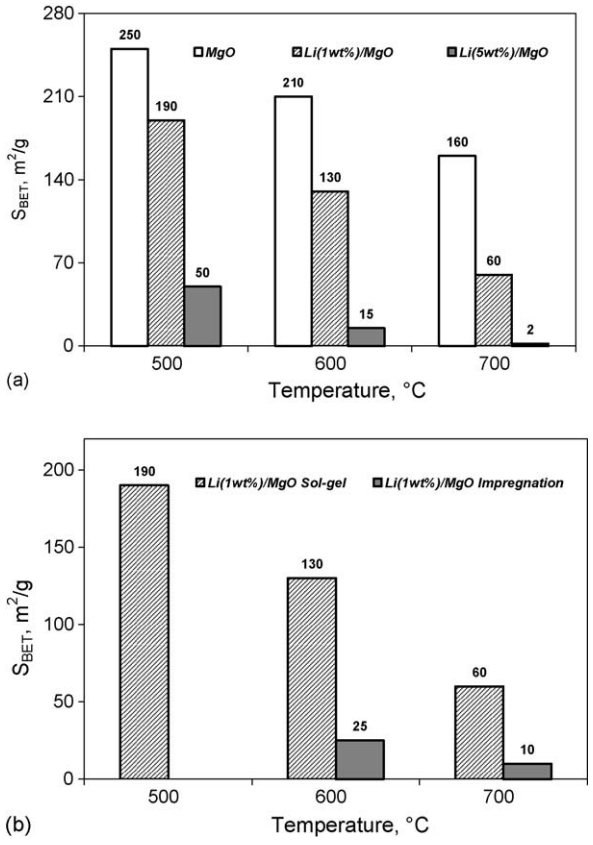

Fig. 8. (a) Surface areas of MgO and Li/MgO samples obtained by sol–gel method after calcination at different temperature; (b) surface area of 1 wt.% Li/MgO obtained by sol–gel method and by conventional impregnation of high surface area MgO after calcinations at different temperature.

3.3. Textural properties of gel and oxide samples

N_2 sorption isotherms were recorded for the dried gels and oxides to study the influence of lithium incorporation on the textural properties of the gel and oxide phases. For Mg-gel and 1 wt.% Li–Mg-gel (Fig. 9) the isotherms are similar and typical for particles possessing mesoporosity (average pore size 3.5 nm, surface area 300 m^2/g). For the 5 wt.% Li–Mg-gel, the surface area was lower (25 m^2/g) and average pore size was much higher (20 nm). The results indicate that the texture of Mg-gel can be retained in the presence of small amounts of Li. At higher Li concentrations the texture is already changed at the gel stage.

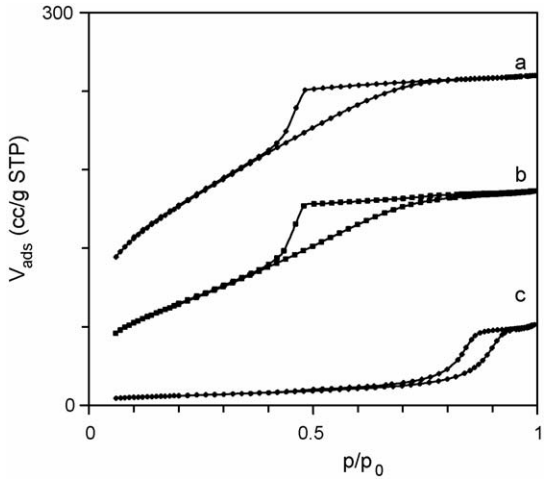

Fig. 9. Nitrogen adsorption isotherms of Mg-gel (a), 1 wt.% Li–Mg-gel (b) and 5 wt.% Li–Mg-gel (c).

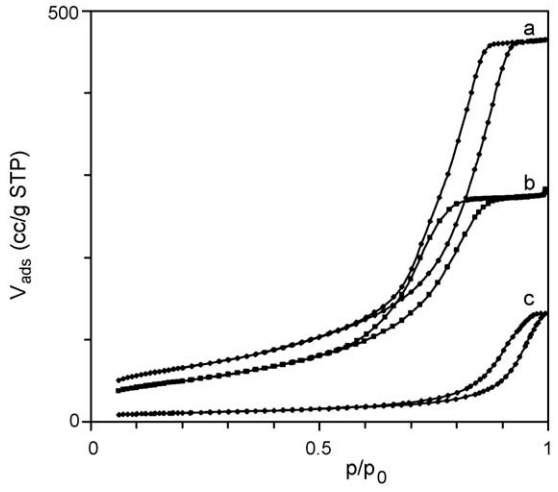

Fig. 10. Nitrogen adsorption isotherms MgO (a), 1 wt.% Li/MgO (b) and 5 wt.% Li/MgO (c) after calcinations at 500 °C.

Fig. 10 shows nitrogen adsorption isotherms for samples calcined at 500 °C. In the case of MgO and 1 wt.% Li/MgO, the hysteresis loop is typical for agglomerates of spherical particles, Type H1 [20]. For the 5 wt.% Li/MgO sample, hysteresis loop was typical for pore structure made by aggregates of platelets, Type H3 [20]. This sample showed an appreciable loss in surface area as described earlier.

TEM photographs for MgO and 5 wt.% Li/MgO are presented in Scheme 1a and b, respectively. It can be seen from the photographs that lithium influences the shape of the oxide aggregates. For MgO a spherical particle shape was observed. About 5 wt.% Li/MgO showed typical cubic particle shape. Cubic particles are usually observed for sintered, crystalline MgO [21].

3.4. Catalytic properties

Catalytic performance in oxidative dehydrogenation of propane in the range of temperature between 500 and 650 °C is compared for 1 wt.% Li/MgO catalysts prepared by sol–gel and conventional wet impregnation (Fig. 11a and b). In the reported experiments propane conversion is below 13% (using high

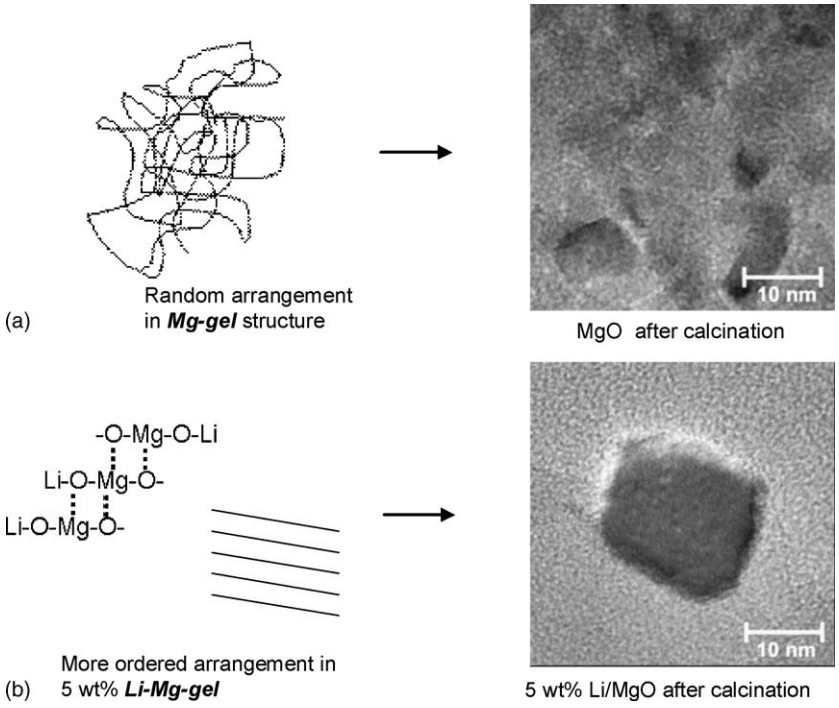

Scheme 1. Different chain length and arrangement at the gel stage: Mg-gel (a), 5 wt.% Li–Mg-gel (b) and resulting oxide material, respectively.

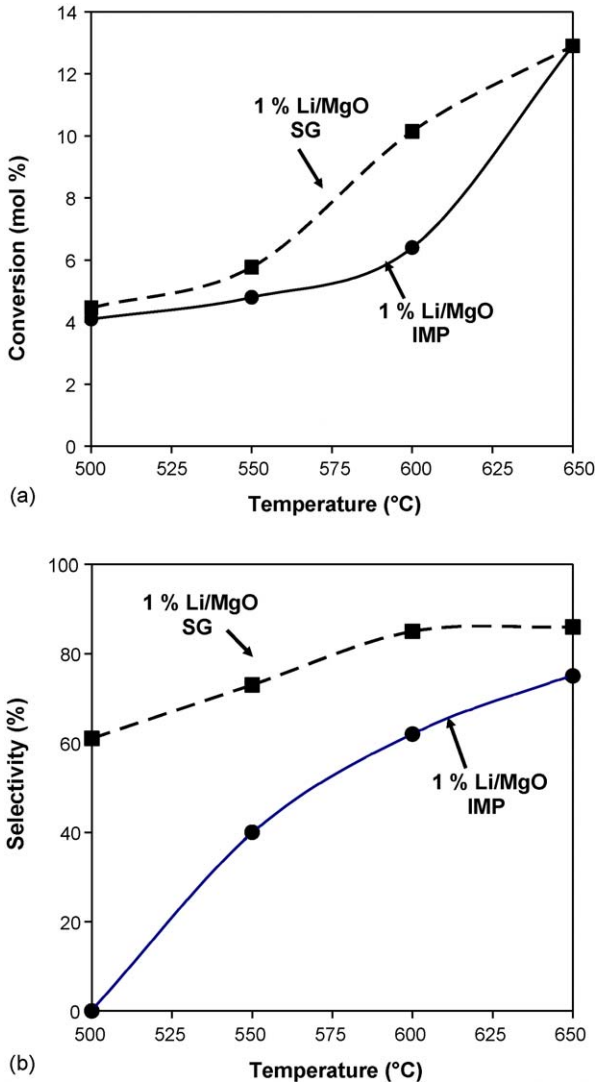

Fig. 11. Oxidative dehydrogenation of propane. Conversion (a) and selectivity to olefins (b) over 1 wt.% Li/MgO catalyst obtained by sol–gel method (SG, square symbols) and conventional impregnation (IMP, round symbols) as function of temperature. Conditions: 10% propane, 10% oxygen, 2% CO_2 and 78% He; GHSV = 120,000 h^{-1}.

space velocity) in order to avoid heat and mass transfer limitation. The sol–gel catalyst gave appreciable higher propane conversion especially at 600 °C. Olefins selectivity in the explored range of temperature is also higher for sol–gel Li/MgO than for conventionally prepared catalyst. Remarkably, at 500 °C sol–gel Li/MgO catalyst presents olefins selectivity (propene and ethene) around 60% while the conventional Li/MgO catalysts show 100% selectivity to complete oxidation (CO_2). Selectivity to olefins increases with temperature in both cases, but sol–gel Li/MgO is always more selective. Moreover, in the case of sol–gel catalyst the main olefin specie formed is propene. Ratio $C^{3=}/C^{2=}$ is always above 1 varying from 4.5 to 1.2 when increasing temperature from 500 to 650 °C. In the case of catalysts prepared by wet impregnation the ratio $C^{3=}/C^{2=}$ is always close to 1. Therefore, the data clearly illustrate the advantage of sol–gel Li/MgO catalysts in propane ODH compared with conventionally prepared catalyst. Detailed testing of the sol–gel Li/MgO catalysts, varying the experimental conditions, Li loading and feed composition are in progress and will be discussed in a subsequent paper.

4. Discussion

4.1. MgO

The sol–gel process involves two main reactions, i.e., hydrolysis and condensation [22]. In the case of Mg-gel obtained from $Mg(OCH_3)_2$ these reactions are

$$Mg(OCH_3)_2 + xH_2O \rightarrow Mg(OH)_x(OCH_3)_{2-x} + xCH_3OH \quad \text{(i)}$$

$$-Mg-(OCH_3) + OH-Mg- \rightarrow -Mg-O-Mg- + CH_3OH \quad \text{(ii)}$$

$$-Mg-OH + OH-Mg- \rightarrow -Mg-O-Mg- + H_2O \quad \text{(iii)}$$

Gel formation can be attributed to presence of: (i) chains of –Mg–O–Mg– bonds (chemical gel) and their internal interaction (Scheme 1) and/or (ii) smaller molecules of $Mg(OH)(OCH_3)$ which interact with each other by hydrogen bonding and/or electrostatic interaction (physical gel) as described in literature (Scheme 2) [16,23]. Our results from thermal analysis and IR spectroscopy indicate partial hydrolysis of the Mg-alkoxide during gel formation.

In the case of partial hydrolysis (e.g., 50% or $x = 1$ in Eq. (i), i.e., formation of $Mg(OCH_3)(OH)$) or complete hydrolysis (100% or $x = 2$ in Eq (i), i.e., formation of $Mg(OH)_2$), one would expect for gel-oxide transformation under thermal treatment weight loss of 44 or 31%, respectively. The experimental weight loss during Mg-gel decomposition to MgO is 34%. From this we can calculate the molecular composition of the Mg-gel to be $Mg(OCH_3)_{0.15}(OH)_{1.85}$ suggesting about 92% hydrolysis. However, other reactions, such as condensation and dehydration (Eqs. (ii) and (iii)) also occur. These reactions cause rejection of methoxy groups (as methanol) or hydroxyls (as water) resulting in oligomers containing –Mg–O–Mg– type species. Observation of the band at 1100 cm^{-1} in IR spectra (Fig. 5), assigned to the bending vibration of Mg–O–Mg bond [17], suggests that both condensation and dehydration occur at the gel stage. The extent of this will determine the amount of –(OH) and –(OCH_3) groups retained in the gel. Three observations indeed confirm

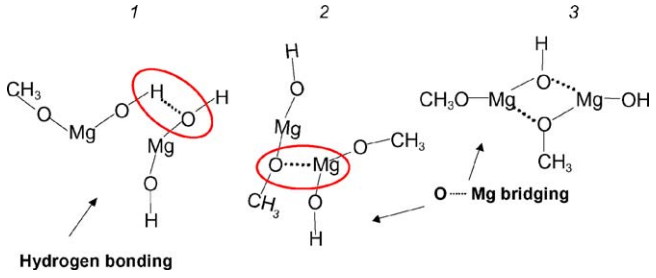

Scheme 2. Examples of interconnected gel molecules of $Mg(OH)(OCH_3)$ through hydrogen bonding (1) or oxygen–magnesium bonding (2 and 3) [18–20].

significant presence of hydroxyl and methoxy groups at gel stage: (i) FTIR experiments show presence of strong methoxy bands in the gel (at 2800 cm^{-1}, Fig. 2), (ii) strong exothermic decomposition of the gel in air and (iii) the large amounts of CO_2 formed during gel combustion (Figs. 3 and 4). Thus, hydrolysis occurs to a much smaller extent than estimated above (92%).

4.2. Li–Mg-gel

The presence of Li ions in the sol–gel system influences the extent of hydrolysis/condensation quite drastically. This can be concluded from the following observations: (i) lower intensity of $–CH_3$ stretching in the IR spectra (Fig. 2c as compared to a), (ii) lower weight loss during calcination for 5 wt.% Li–Mg gel (24%) versus Mg-gel (34%) and (iii) lower amounts of CO_2 formed during combustion. These observations suggest that Li ions definitely enhance hydrolysis. Thus, the presence of Li ions changes the composition of the gel. Difference in the gel structure is also confirmed by N_2 adsorption isotherms shown in Fig. 9, demonstrating that Mg-gel is typically mesoporous whereas 5 wt.% Li–Mg-gel contains macropores.

Thus, addition of lithium precursor seems to generate a different ordering in the gel, as also supported by the fact that the isomorphic transition observed at 210 °C for the Mg-gel is absent in the case of Li–Mg-gels. Reller and co-workers [24] qualitatively, attributed this transition for magnesia gel to either (i) a re-crystallization or (ii) formation of a new phase by intermediate species containing bridging of OH groups as shown in Scheme 2, case 1. The exact nature of these structures are neither relevant to this study nor taken up for further discussion, but the fact that such a transition is absent when Li ions are present in the gel confirms that the ordering in the presence of Li ions is different.

It is thus likely that lithium ions are incorporated already in magnesia at Li–Mg-gel stage. The incorporated lithium can be directly bound in magnesium gel structure and located as a terminating entity (–Mg–O–Li). A consequence of this is that the presence of lithium as a terminating entity will prevent further condensation and chain growth as shown in Scheme 3. Moreover, chain termination by Li as –Mg–O–Li instead of –Mg–OH or $–Mg–OCH_3$ decreases the presence of hydroxyl or methoxy groups as observed in Fig. 2.

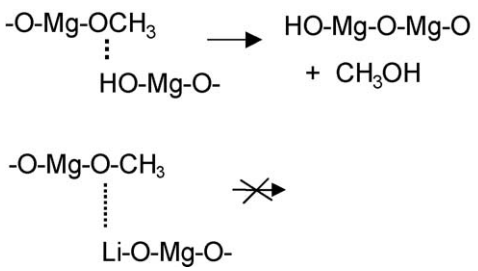

Scheme 3. Role of lithium, terminating chain at the gel stage during condensation reaction and chain growth.

4.3. Li/MgO oxide

Samples containing 1 wt.% Li/MgO obtained by sol–gel route posses low amount of free Li (about 0.6 wt.% Li) and maintain high surface area even after treatment at higher temperatures (190 m^2/g, see Fig. 8a). This indicates that small amounts of Li, even when present as free phase of Li_2CO_3, are not detrimental for making high surface area Li/MgO catalysts. The sol–gel method applied to Li/MgO materials synthesis achieves two objectives simultaneously: (i) allows incorporation of Li in the magnesia under milder conditions during gelation and (ii) minimizes sintering during thermal treatments. The approach is less successful in the case of the 5 wt.% Li containing sample. In this sample free Li carbonate phase (about 4.2 wt.% Li) is present and, as expected, the oxide formed on calcinations at 500 °C has a relatively low surface area (50 m^2/g). The effect of Li assisted sintering is also seen from the nitrogen sorption curves: MgO and 1 wt.% Li/MgO show typical mesoporosity and high surface area whereas, the hysteresis loop for 5 wt.% Li/MgO material indicates more macro-porosity.

Calcination of Mg-gel gives rise to presence of spherical like particles as observed by TEM. Extensive condensation and chain growth at the gel stage in the absence Li may lead to more random agglomerates and spherical type structures. On the contrary, short chains, formed in the presence of Li, tend to form a more ordered gel structure giving rise to cubic Li/MgO particles after calcination. A qualitative representation is shown below in Scheme 1. However, in this case due to the presence of Li, we cannot rule out that enhanced sintering is responsible for the observed changes in the particle shape [25].

Preparation of Li/MgO catalysts by conventional method (impregnation of bulk MgO with Li salts) leads to the formation of mixture of phases of Li_2CO_3 and MgO [26]. This is because Li_2O formed on calcinations easily sorbs CO_2 from atmosphere and forms Li_2CO_3. Only a high temperature treatment allows the incorporation of lithium (Li_2CO_3 melts/decomposes around 750 °C) because it makes possible for Li^+ ions to diffuse into the MgO lattice replacing Mg^{2+} ions. The disadvantage of this is that this mobility of the Li species and high T facilitate sintering of MgO and subsequent loss of surface area. This is also seen clearly from Fig. 8b. The high surface area MgO (250 m^2/g) is drastically reduced on impregnation with $LiNO_3$ and subsequent calcinations at 600 and 700 °C (1 wt.% Li/MgO, respectively, 25 and 10 m^2/g).

Both catalytic activity and selectivity in ODH of propane of the sol–gel catalyst are superior in comparison with Li/MgO prepared by conventional impregnation. This is probably the result of two effects: (i) the sol–gel derived catalyst has a significant higher surface area (130 m^2/g versus 25 m^2/g) and (ii) the sol–gel derived catalyst contains a higher amount of Li incorporated in the MgO matrix. Both effects contribute to an increase in the number of active sites, i.e., $[Li^+O^-]$. A third effect may contribute as well: the number of low-coordination sites is increasing when decreasing the size of the primary particles, and when lithium is incorporated and this could well influence the generation and/or properties of $[Li^+O^-]$ sites on

the surface. In future work we will study this effect with IR spectroscopy of CO adsorbed at low temperatures. The observed effect on activity is not very surprising. However, the effect on selectivity is not obvious at all taking into account the complex mechanism of catalytic ODH process, which includes radical generation at the active site in combination with radical chain reactions in gas-phase as well as quenching reactions on the catalyst surface [11].

The catalysts obtained have sufficient thermal stability for application in oxidative dehydrogenation and cracking as the operation temperature is typically below 650 °C, in contrast to the classical application of Li/MgO catalysts for the oxidative coupling of methane at much higher temperatures (750–800 °C).

5. Conclusions

High surface area nanoscale Li/MgO oxide clusters can be synthesized by sol–gel method, co-gelling $Mg(OCH_3)_2$ and $LiNO_3$ in methanol/water solution followed by drying at 50 °C under vacuum and calcination at 500 °C in air. Lithium ions are incorporated in the magnesia structure already at the gel stage, probably enhancing formation of $[Li^+O^-]$ type active sites at relatively low temperatures. Moreover, the enhanced lithium incorporation can result also in an increased number of low coordinated sites. At this stage we cannot rule out any influence of low coordinated sites on the catalytic activity. When the Li loading is low (1 wt.%), the structural and textural characteristics of the magnesia gel and eventually magnesium oxide are not significantly affected; the resulting Li/MgO retains high surface area and mesoporosity. At higher Li loading, the characteristics of the gel are changed: the gel is more ordered.

The sol–gel procedure allows significant incorporation of Li ions at temperatures below 650 °C, i.e., temperature at which Li ions are not incorporated at all in impregnated Li/MgO catalysts. Consequently, less Li_2CO_3 is present in sol–gel derived catalysts during calcination. This effect is responsible for both high surface area obtained after calcination as well as for enhanced thermal stability of Li/MgO. Sol–gel derived Li/MgO provides significantly higher olefin yields in ODH of propane in comparison with conventional Li/MgO catalysts. Olefins dominate even at 500 °C when catalysts by wet impregnation produce only CO_2.

Sol–gel derived Li/MgO is a very promising catalyst for the oxidative dehydrogenation of propane to olefins.

Acknowledgements

The authors would like to thank L. Vrielink for XRF-analysis and nitrogen sorption measurements, M. Smithers for TEM recordings and H. Koster for XRD studies. We thank CW/NWO, The Netherlands for financial support (project number 700.50.005).

References

[1] C. Shi, M. Xu, M.P. Rosynek, J.H. Lunsford, J. Phys. Chem. 97 (1993) 216–222.
[2] M.A. Johnson, E.V. Stefanovich, T.N. Truong, J. Phys. Chem. B 101 (1997) 3196–3201.
[3] L. Lefferts, K. Seshan, B. Mojet, J.G. van Ommen, Catal. Today 100 (2005) 63–69.
[4] E.A. Mamedov, V. Cortes Corberan, Appl. Catal. A 127 (1995) 1–40.
[5] F. Cavani, F. Trifiró, Catal. Today 24 (1995) 307–313.
[6] M.V. Landau, M.L. Kaliya, M. Herskowitz, P.F. van den Oosterkamp, P.S.G. Boque, Chemtech 26 (2) (1996) 24–29.
[7] M. Herskowitz, M. Landau, M. Kaliya, US Patent 6,130,183 (October 2000).
[8] S. Zender, Hydrocarbon Process. 77 (2) (1998) 59–65.
[9] J.H. Lunsford, Adv. Catal. 35 (1987) 139.
[10] J.X. Wang, J.H. Lunsford, J. Phys. Chem. 90 (1986) 5883–5887.
[11] L. Leveles, K. Seshan, J.A. Lercher, L. Lefferts, J. Catal. 218 (2003) 307–314.
[12] T. Ito, J.X. Wang, C.H. Lin, J.H. Lunsford, J. Am. Chem. Soc. 107 (1985) 5062–5068.
[13] K.J. Klabunde, J. Stark, D. Zhang, J. Phys. Chem. 100 (1996) 12142–12153.
[14] L. Leveles, Ph.D. Thesis, University of Twente, The Netherlands, 2002.
[15] J.A. Roos, S.J. Korf, R.H.J. Veehof, J.G. van Ommen, J.R.H. Ross, Appl. Catal. 52 (1989) 147–156.
[16] Y. Diao, W.P. Walawender, C.M. Sorensen, K.J. Klabunde, T. Ricker, Chem. Mater. 14 (2002) 362–368.
[17] T. Lopez, R. Gomez, A. Ramirez-Solis, E. Poulain, O. Novaro, J. Mol. Catal. 88 (1994) 71–84.
[18] J.L. Boldú, E. Munoz, X. Bokhimi, O. Novaro, Langmuir 15 (1999) 32–35.
[19] R.C. Weast, Handbook of Chemistry and Physics, 64th ed., CRC Press Inc., Florida, 1984, pp. B106–B108.
[20] K.S. Sing, Pure Appl. Chem. 57 (4) (1985) 612.
[21] J. Hargreaves, G. Hutchings, R.W. Joyner, C. Kiely, J. Catal. Today 13 (1992) 401–407.
[22] C.J. Brinker, Sol Gel Science, Academic Press, New York, 1990, p. 108 (Chapter 3).
[23] R. Portillo, T. Lopez, R. Gomez, A. Morales, O. Novaro, Langmuir 12 (1996) 40–44.
[24] H. Thoms, M. Epple, H. Viebrock, A. Reller, J. Mater. Chem. 5 (4) (1995) 589–594.
[25] A.G. Andersen, T. Norby, Catal. Today 6 (1990) 575–586.
[26] X.D. Peng, D.A. Richards, P.C. Stair, J. Catal. 121 (1990) 99–109.